 Nucleic Acids Research, 1999, Vol. 27, No. 22 **4353–4362**

Characterization of transient RNA–RNA interactions important for the facilitated structure formation of bacterial ribosomal 16S RNA

Willi Besançon and Rolf Wagner*

Institut für Physikalische Biologie, Heinrich-Heine-Universität Düsseldorf, Universitätsstraße 1, D-40225 Düsseldorf, Germany

Received August 16, 1999; Revised and Accepted September 27, 1999

ABSTRACT

The co-transcribed leader sequences of bacterial rRNA are known to affect the structure and function of the small ribosomal subunits. Base changes in the leader *nut*-like sequence elements have been shown to cause misfolded but correctly processed 16S rRNA structures at low growth temperature. Transient interactions of leader sequences with the nascent 16S rRNA are considered to guide rRNA folding and to facilitate correct structure formation. In order to understand this chaperone-like activity of the leader RNA we have analyzed the thermodynamic stabilities of wild-type and mutant leader transcripts. We show here that base changes cause subtle differences in the melting profiles of the corresponding leader transcripts. Furthermore, we show that direct interaction between leader transcripts and the 16S rRNA is limited to the 5′-domain of the 16S rRNA for both wild-type and mutant leaders. Binding studies of mutant and wild-type leader transcripts to 16S rRNA revealed small changes in the affinities and the thermal stabilities as a consequence of the base changes. Different complex stabilities as a function of the Mg^{2+} ion concentration indicated that mutant and wild-type leader transcripts interact differently with the 16S rRNA, consistent with a less stable and tightly folded structure of the mutant leader. Employing time-resolved oligonucleotide hybridization assays we could show different folding kinetics for 16S rRNA molecules when linked to wild-type leader, mutant leader or in the absence of leader RNA. The studies help to understand how bacterial rRNA leader transcripts may affect the folding of the small subunit rRNA.

INTRODUCTION

Ribosomal RNAs (rRNAs) are important constituents of the protein synthesizing machinery. They are the most intensively transcribed RNAs in bacterial cells and their complex regulation determines to a large extent balanced adaptation of the protein synthesizing capacity to growth demands (1). Generally, rRNAs are transcribed as contiguous precursor molecules with leader and spacer sequences flanking the structural genes. The leader and spacer regions are removed by an ordered processing pathway and they are not present in the final ribosome particles (2,3). A number of important functional elements have been recognized within leader and spacer sequences, consistent with the high degree of sequence conservation (4,5). These sequences do not contain only the recognition sites necessary for their correct removal. The additional presence of *nut*-like sequences is considered to function as signals to suppress premature transcription termination. Moreover, these sequence elements have recently been shown to participate in a new function that was not previously known for RNA molecules. The highly conserved leader regions, and most likely also the spacer sequences, participate actively in the rRNA folding process facilitating ribosome biogenesis (4,6,7). The function of rRNA leaders has therefore been compared with those of molecular chaperones which assist correct ribosome formation. This has been shown specifically for *Escherichia coli* where rRNA leaders have the capacity to interact with defined regions of the growing 16S rRNA transcript before they are removed by processing nucleases. A chaperone-like function of leader sequences in guiding correct rRNA folding is supported by certain mutations within the highly conserved leaders, which result in structurally and functionally defective 30S particles (8). The nature of the structural aberrations of such particles has been determined by a systematic analysis of ribosomes from mutant and wild-type cells *in vivo* employing chemical probing techniques (8). Because the protein composition and the processing steps of assembled particles from such mutants appear to be normal these findings support the conclusion that the leader RNA assists correct folding and structure formation of the small ribosomal subunit through transient interactions with the nascent rRNA transcript. Since mutations in the leader rRNA cause a cold-sensitive phenotype the activity facilitating rRNA folding is probably most important under suboptimal growth conditions, e.g. at low temperature. It is feasible that transient leader RNA–16S rRNA interactions prevent the formation of unfavorable structures which might

*To whom correspondence should be addressed. Tel: +49 211 811 4928; Fax: +49 211 811 5167; Email: r.wagner@mail.rz.uni-duesseldorf.de
Present address:
Willi Besançon, Novartis Pharma GmbH, Roonstraße 25, D-90429 Nürnberg, Germany

form as metastable intermediates of the nascent transcript, causing irreversibly misfolded conformations. Alternatively, the correct folding pathway may be directed by a facilitator function of the leader sequence. Since the leader also contains target sites for interaction with specific proteins (e.g. Nus factors and the small ribosomal subunit protein S10) it may in addition support initiation of the protein assembly pathway.

In this study we have performed an *in vitro* analysis to better understand the dynamic function of the bacterial leader RNA. Transcripts were used that corresponded to the leader sequences of a pair of mutants characterized previously (23). The T0 mutant has the *rrnB* wild-type sequence with the exception of a single A→G base change at position 239, relative to the transcription start at rRNA promoter P1. This mutant does not show a measurable phenotype and the corresponding transcript is therefore designated 'wild-type' in this study. The T11 transcript corresponds to the T11 mutant and deviates from the T0 sequence at two positions (C262 and C274 are both changed to U). These base changes confer a cold-sensitive phenotype with severe growth retardation at low temperature. Experiments were designed to answer the following questions: (i) what is the nature of the leader RNA–16S rRNA interaction; (ii) can we characterize the major step(s) where the correct folding pathway of the 16S rRNA depends on a transient leader RNA contact?

The results show that specific interactions of the ribosomal leader RNA occur only with sequence elements of the 16S rRNA 5′-domain. This interaction is of transient nature since it is readily competed by a stable complex between the leader and sequences flanking the 16S rRNA 3′-end. This structure is known to constitute the RNase III processing site (9). Wild-type and mutant leader RNAs differ slightly in their binding affinities to 5′ 16S rRNA fragments, indicating subtle structural differences. These structural differences are reflected in different melting profiles for wild-type and leader transcripts which contain base change mutations. Analysis of the 16S rRNA folding kinetics, starting from denatured transcripts, revealed significant differences for several internal 16S rRNA secondary structural elements depending on the presence of the leader or on mutations within the leader. Together the results support the chaperone-like activity of the rRNA leader and help our understanding of the pathway induced by certain leader mutations that cause defective 30S particles.

MATERIALS AND METHODS

Strains, enzymes and chemicals

Escherichia coli strains HB101 and GM2199 (10,11) were used as hosts for plasmid constructions and plasmid preparations. GM2199 was used to obtain plasmid DNA free of methylation.

Polynucleotide kinase and G50 Sephadex spin columns were obtained from Boehringer (Germany). T7 RNA polymerase was a kind gift of B. Esters. Standard methods for DNA manipulation were used throughout (12). Radioactive nucleotides were purchased from Hartmann (Germany).

Plasmids

Ampicillin resistant (Amp^r) plasmids pLT7P2, pLT7P2-0 and pLT7P2-11, containing the wild-type or the mutant *rrnB* leader regions under the control of the T7 promoter, have been described previously (13). Plasmid pLT7P2-0 is a derivative of pLT7P2-11. It contains an A→G base transition in the *rrnB* leader sequence at position +239 relative to the transcription start at rRNA promoter P1. Transcripts derived from this vector are designated as T0 mutant transcripts. The plasmids pWB and pWB-11 were used as templates for T7 RNA polymerase *in vitro* transcription to obtain large amounts of 16S RNA run-off transcripts with the wild-type or the mutant T11 *rrnB* leader regions, respectively. For the construction of pWB the plasmid pBP2, a pUC19 derivative of p7-16S (14), was digested with *Sac*I and *Bcl*I. A 256 bp *Nae*I–*Bcl*I fragment derived from pLT7P-2 was inserted to obtain pWB. To obtain plasmid pWB-11 the parental plasmid pBP2 was digested with *Kpn*I and *Bcl*I and a 227 bp *Kpn*I–*Bcl*I fragment from p7P2-11 was inserted. The plasmid p7-1231 contains a 640 bp *Dra*I–*Pml*I fragment from pKK3535 (15) encoding the 3′-terminal 311 nt of the 16S rRNA ligated into the *Dra*I + *Pml*I-opened pUC18-T7 (13). For the isolation of RNA containing the central domain of the 16S rRNA (positions 418–1230) the plasmid p7-16M was constructed. This vector contained the 813 bp *Stu*I–*Pml*I fragment from pBP2 inserted into a *Stu*I-linearized pUC18-T7 plasmid. The different plasmids are summarized in Table 1.

Run-off transcription from linearized templates

The plasmids with different portions of the *rrnB* operon cloned under the control of the phage T7 promoter were used as templates for *in vitro* transcription. Specific run-off transcripts were obtained after linearization of the vectors with different restriction enzymes. A list of the different template vectors, the respective restriction enzymes for linearization, and the length of the resulting transcripts is presented in Table 1. *In vitro* transcription was performed with purified T7 RNA polymerase as described (16). Transcripts were purified by gel electrophoresis in the presence of 7 M urea or on Sephadex G50 spin columns. To obtain statistically labeled radioactive transcripts *in vitro* transcription reactions were performed in the presence of 10–50 μCi [α-^{32}P]UTP. RNA concentrations were determined spectrophotometrically at 260 nm or by taking advantage of the specific radioactivity of the purified transcripts.

RNA–RNA complex formation

Binding of rRNA leader transcripts to fragments of the 16S rRNA was tested in the following way. Between 1 and 4 pmol ^{32}P-labeled 16S rRNA fragments were mixed with varying amounts (0.1–60 pmol) of unlabeled rRNA leader transcripts in 10 μl 20 mM Na cacodylate, pH 7.2, 100 mM KCl, 1 mM EDTA and $MgCl_2$ as indicated. The mixture was incubated for 3 min at 70°C, followed by slow cooling to 4°C (1°C/min). Samples were analyzed by gel electrophoresis on 5% polyacrylamide gels in a buffer containing 40 mM Tris–OAc, pH 7.5, 20 mM Na borate, 2 mM EDTA. Separation was performed at 200 V for 20 h at 4°C. Gels were subjected to autoradiography and the amounts of complexes and free nucleic acids were determined after densitometric evaluation of the corresponding bands of the autoradiograms.

Temperature gradient gel electrophoresis

The thermodynamic stability of leader RNA–16S rRNA complexes was determined taking advantage of temperature gradient gel electrophoresis (TGGE) (17). Samples were separated after complex formation on 5% native polyacrylamide gels with a continuous temperature gradient from 10 to 25°C. Gels

Table 1. Templates and transcripts

Plasmid	Restriction enzyme	Run-off transcript	Length of the transcript (nt)
pLT7P2	*Dra*I	Wild-type leader	173[a]
pLT7P2-0	*Dra*I	pT0 leader	173[a]
pLT7P2-11	*Dra*I	pT11 leader	173[a]
pBP2	*Bst*EII	16S RNA 1–1504	1506[b]
pBP2	*Sca*I	16S RNA 1–434	436[b]
p7-16M	*Bam*HI	16S RNA 418–1230	819[c]
p7-1231	*Bst*EII	16S RNA 1231–1504	275[b]
p7-1231	*Xba*I	16S RNA (1231–1542)–3′ 16S RNA spacer	494[b]
pWB	*Bst*EII	Wild-type leader–16S RNA	1677[b]
pWB-11	*Bst*EII	pT11 leader–16S RNA	1677[b]

[a]The sequences start at the 5′-end with GG instead of the natural sequence GC.
[b]Sequences start with GGGG at the 5′-end.
[c]Sequences have five non-ribosomal RNA nucleotides at their 3′-end.

were silver stained after separation and temperatures were determined at which half of the complexes had been thermally dissociated.

Oligonucleotides

Oligonucleotides for hybridization were 5′-end-labeled with [γ-^{32}P]ATP and T4 polynucleotide kinase to a specific radioactivity of 1000 Ci/mmol. Oligonucleotides complementary to sequence regions within defined helices of the 16S rRNA secondary structure [number of helices according to Brimacombe *et al*. (18) are given in parentheses] were used: 1, positions 25–38 (helix 3); 2, positions 66–82 (helix 6); 3, positions 163–177 (helix 8); 4, positions 481–494 (helix 17); 5, positions 503–517 (helix 18); 6, positions 572–587 (helix 20); 7, positions 962–978 (helix 31); 8, positions 1419–1437 (helix 44).

16S rRNA oligonucleotide binding assay

The hybridization kinetics of radioactive oligonucleotides to specific regions of the 16S rRNA structure were used to monitor the rate of 16S rRNA secondary structure formation. The experiments performed were an adaptation of a procedure described recently (19). Starting with heat-denatured 16S rRNA the time course of oligonucleotide binding to specific domains of the renaturing 16S rRNA molecule was determined by following 16S rRNA–oligonucleotide complex formation. The amounts of complexes formed were quantified after gel electrophoresis of the resulting binary complexes on native polyacrylamide gels. Briefly, non-radioactive 16S RNA (0.5 pmol) was heated at 90°C for 2 min in 10 µl annealing buffer (50 mM Tris–HCl, pH 8.5, 100 mM KCl) and rapidly cooled to 37°C. At different renaturing times (0–120 s) 5 pmol (in 5 µl annealing buffer) of a pre-warmed radioactive oligonucleotide, complementary to a specific secondary structural region of the 16S rRNA, was added to an aliquot of the 16S RNA sample. After 20 s annealing time at 37°C the samples were cooled on ice for 30 s, mixed with an equal volume of 40 mM Tris–acetate, pH 7.5, 20 mM Na-borate, 2 mM EDTA, 30% glycerol (0°C) and immediately subjected to gel electrophoresis on composite 1% agarose–3% acrylamide gels. Electrophoresis was performed in 40 mM Tris–acetate, pH 7.5, 20 mM Na-borate, 2 mM EDTA at 4°C. Gels were subsequently autoradiographed and hybridization signals were quantified according to densitometric evaluation of band intensities.

Determination of optical melting curves

RNA samples for UV melting experiments were generally purified by G50 gel filtration. Routinely 0.5 A_{260} units of RNA in 100 µl melting buffer (1 mM Na-cacodylate, 0.1 mM EDTA, with varying concentrations of K^+ or Na^+ between 10 and 500 mM). Magnesium concentration was set as indicated. A modified Sigma ZWS II spectrophotometer was used to collect absorbance data at 260 and 280 nm as a function of temperature (20). Heating and cooling rates were 0.25°C/min. Cooling curves were routinely taken to check for reversibility of the melting curves.

RESULTS AND DISCUSSION

Effect of base change mutations on the leader RNA secondary structure

A secondary structure model of the wild-type rRNA leader based on limited enzymatic hydrolysis and chemical modification studies has been presented recently (13). The same study revealed subtle changes in the secondary or higher order structure when base changes were present in the leader. The same base changes caused a cold-sensitive phenotype when expressed in cells (23). The structural differences were apparent only at low temperature indicating that the leader must be able to exist in several interconvertible conformations. In fact, two such conformations with a transition temperature between 10 and 15°C have been detected by TGGE (13). Here we have extended the analysis and examined the wild-type and the T11 mutant leader transcript containing base changes at positions 239 (A→G), 262 (C→U) and 274 (C→U), relative to the genuine rRNA promoter P1 transcription start site. Leader transcripts (173 nt in length; Table 1) were analyzed by a UV

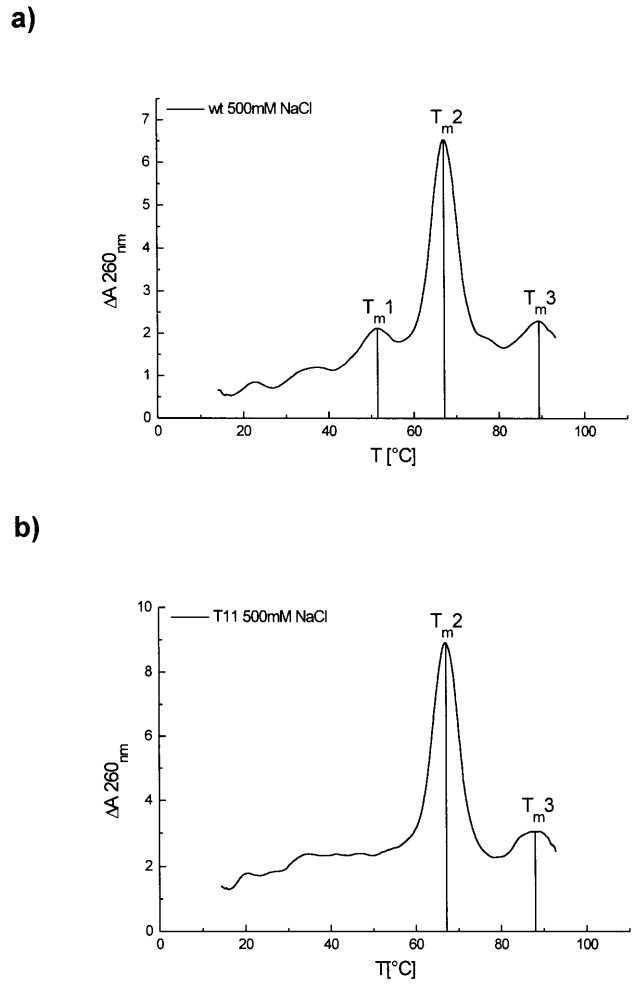

Figure 1. UV melting analysis of wild-type and T11 mutant leader transcripts. The differentiated melting profiles obtained for the 173 nt leader RNA transcripts in the presence of 500 mM NaCl are shown. (**a**) Wild-type leader RNA; (**b**) pT11 leader RNA. The melting transitions are indicated by T_m1, T_m2 and T_m3, respectively.

melting study following the temperature-dependent change in hyperchromicity (Materials and Methods). As can be seen in Figure 1a, temperature-dependent melting of the wild-type leader occurs in three distinct steps, with one major and two minor transitions. The T_m values at 500 mM monovalent salt concentration are 67°C for the major transition (T_m2) and 52 (T_m1) and 89°C (T_m3) for the two minor transitions, respectively. Comparison of the respective melting profile for the T11 mutant leader transcript (Fig. 1b) reveals that the lowest transition (T_m1) is missing. We have examined the dependence of the transition temperatures on salt concentration ranging from 10 to 500 mM and found a linear relationship for all transitions with ~16°C difference per 10-fold change in the monovalent ion concentration. Extrapolation to the ionic strength that prevails under TGGE electrophoresis conditions yielded excellent agreement with the temperature transitions detected in previous TGGE experiments (13).

The UV melting data were further analyzed with the program POLAND (21) and compared with theoretical melting curves obtained according to the program LinAll (20,22). These theoretical melting profiles predict a similar difference between the wild-type and the T11 mutant leader transcripts. Three transitions (one major and two minor) were proposed. The lowest transition for the T11 mutant is shifted to an ~10°C lower temperature compared to the wild-type. The data was used to predict secondary structures with decreasing stabilities for the different transcripts, which could be correlated to the different transition temperatures. The predicted arrangement of secondary structural elements is in very good agreement with the experimentally determined structure (13). Several different structures can be derived for the wild-type and the T11 mutant at low temperature which would account for the difference in melting (data not shown).

Taken together, the UV melting analysis reveals that base changes in the leader t_L region cause a difference in the secondary structure between the wild-type and mutant RNA molecules which is in accord with the previous TGGE analysis and may be the underlying cause for the temperature-dependent phenotype conferred by leader mutations.

Complex formation between leader RNA and 16S rRNA

Next we asked the question whether the different leader RNA molecules could interact in a different way with the 16S rRNA. Binding and cross-linking experiments have shown in previous studies that the leader RNA has the capacity to interact with mature 16S rRNA. The *nut*-like sequence elements (boxA, boxB and boxC) and the t_L region were identified as interacting sites and several positions within the 16S rRNA 5′-domain were identified at the nucleotide level as sites that are in close contact with the leader when both molecules form a complex (13,16). It is supposed that this interaction guides the correct folding path and facilitates the maturation and assembly process. Because the t_L mutations in the leader cause an aberrant 16S rRNA structure and structurally and functionally defective 30S particles (8) we were interested to answer the following questions: (i) are there additional contact regions between the leader and the 16S rRNA molecules at sites other than the 5′-domain, which had been identified by the cross-linking study; (ii) do mutations in the leader t_L sequence, which cause subtle structural differences at low temperature, affect the site(s) or affinity of the leader–16S rRNA interaction?

To examine whether the wild-type and T11 mutant leader transcripts were able to interact with the 16S rRNA at sites further downstream of the first 370 nt from the 5′-end, where the cross-linking sites had been mapped, we took advantage of a gel retardation assay employing ^{32}P-labeled 16S rRNA transcripts of different length and various leader transcripts. The following 16S fragments were used for complex formation (Table 1): a 436 nt 5′-terminal fragment containing the 16S sequence positions 1–434; a 819 nt central fragment comprising positions 418–1230; a 275 nt 3′-terminal fragment containing the sequence 1231–1504. Three different leader transcripts (173 nt in length; Table 1) were compared for complex formation: the wild-type leader; the T11 mutant leader (base changes at positions 239, 262 and 274); the T0 mutant leader, which contains a single base change (A→G at position 239) that does not cause a phenotype when expressed in transformed cells. Complex formation was performed under standard conditions (Materials and Methods) with increasing leader concentrations up to a 60-fold molar excess of leader over 16S rRNA fragments.

Table 2. Thermodynamic parameters of RNA–RNA complex formation[a]

Leader RNA	K_{Bobs} (M^{-1})		ΔG (kJ/mol)	
	5′ 16S rRNA	3′ 16S spacer	5′ 16S rRNA	3′ 16S spacer
Wild-type	$0.6 \pm 0.2 \times 10^5$	$5.0 \pm 2.5 \times 10^6$	–25.3	–35.5
T11	$2.5 \pm 0.3 \times 10^5$	$1 \pm 1.1 \times 10^7$	–28.6	–37.1
T0	$1.8 \pm 1.1 \times 10^5$	$1 \pm 1.1 \times 10^7$	–27.9	–37.1

[a]Complexes were analyzed in the presence of 1 mM Mg^{2+}.

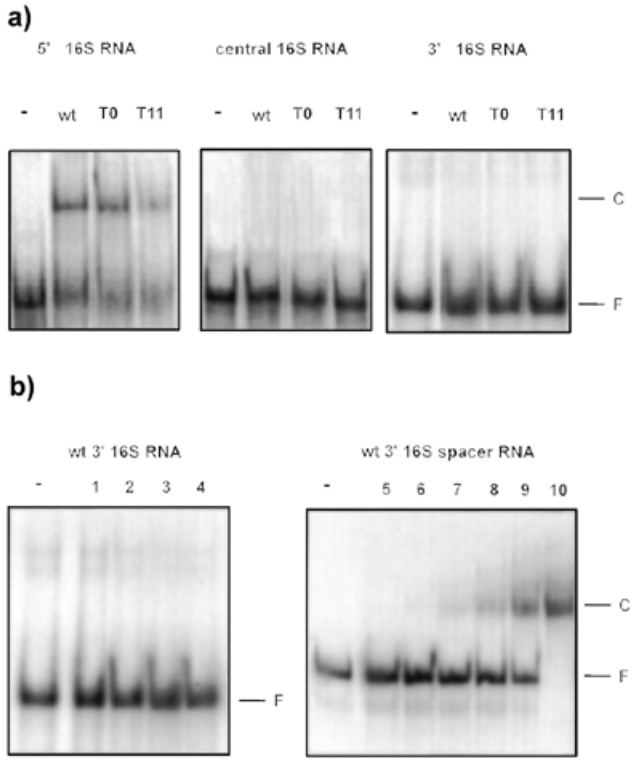

Figure 2. Identification of the 16S rRNA fragments involved in complex formation with leader transcripts. Complex formation was performed with 100 nM radiolabeled 16S rRNA fragments and 6 µM leader transcripts. (**a**) 5′ 16S RNA represents a 436 nt transcript containing the 16S rRNA sequence positions 1–434. Central 16S RNA corresponds to a 819 nt transcript with 16S rRNA positions 418–1230. 3′ 16S RNA represents a 275 nt fragment with the 16S rRNA sequence positions 1231–1504. C indicates the position of the leader RNA–16S rRNA complex; F denotes the position of the free 16S rRNA fragment. The presence of the different leader transcripts is indicated by wt, T0 and T11 as wild-type, T11 and T0 mutant, respectively. (**b**) Wild-type 3′ 16S RNA represents binding analysis of the 275 nt 16S rRNA fragment (positions 1231–1504) with the wild-type leader transcript. Wild-type 3′ 16S spacer RNA represents the binding study with a 494 nt 16S rRNA fragment that contains the last 311 nt of the mature 16S rRNA plus 183 nt of the 3′-flanking spacer. The following concentrations of wild-type leader transcripts were employed for complex formation: no leader (indicated by –) and 1 (lane 1), 2 (lane 2), 4 (lane 3), 6 (lane 4), 0.01 (lane 5), 0.02 (lane 6), 0.05 (lane 7), 0.1 (lane 8), 0.2 (lane 9) and 0.4 µM (lane 10).

As can be seen in Figure 2a, stable complex formation can only be observed between leader transcripts and the 5′-fragment of the 16S rRNA. Apparently, all leader transcripts tested are able to interact. Comparison of the gel mobilities of the various complexes did not indicate any conformational differences when different leader transcripts were employed.

It is known that during the folding and processing pathway of ribosomal primary transcripts a stable stem structure between sequences flanking the 3′-end of the 16S rRNA (the spacer region) and the leader RNA are formed. This structure contains the RNase III processing site and its formation is a prerequisite for the first processing cut by RNase III (9). Since neither processing at the 3′- nor 5′-end of the 16S rRNA precursor is affected by the T11 mutation (23) we wished to examine whether formation of the processing stem can be affected by the leader RNA–16S rRNA interaction. Complex formation was therefore repeated between the different leader transcripts and a 494 nt 16S rRNA transcript that additionally contained 180 nt downstream of the mature 3′-end (Table 1). The results of such binding studies for the wild-type leader are shown in Figure 2b. It can be seen that a strong complex is formed. Note that the presence of the 16S rRNA 3′-extension causes complete complex formation with the leader transcript while the 16S rRNA without the 3′-extension does not yield detectable amounts of complex, even at a 10-fold higher leader transcript concentration (Fig. 2b, compare lanes 3 and 10). No quantitative differences in complex formation could be detected when T11 or T0 mutant leader transcripts were used. These results support the observation that interaction between the leader and the 16S rRNA 5′-domain must be of a transient nature and does not notably disturb subsequent formation of the RNase III processing stem. The results are furthermore in accord with the finding that the T11 mutation does not cause aberrant processing of 16S rRNA (23).

If there is no qualitative difference in the interaction of wild-type and mutant leader transcripts with the 5′-domain of the 16S rRNA it could still be possible that the affinities of the different transcripts for 16S rRNA might be affected. To compare binding affinities between different leader transcripts and the 16S rRNA on a more quantitative basis we determined the apparent binding constants according to densitometric evaluation of retardation gels when complex formation was studied at different leader concentrations (24). The results are summarized in Table 2, where binding constants are presented for complexes between the 16S rRNA 5′-fragment and wild-type as well as T0 and T11 mutant leader transcripts. There is a notable but not a dramatic difference visible between the wild-type and the T11 mutant, which shows an ~4-fold stronger binding. There are no significant differences detectable, on the other hand, for the different leader transcripts and the 16S rRNA fragment that contains part of the 3′-spacer sequence.

In addition to the binding constants, which can be taken as a measure of affinity, we have determined the thermal stability of the complexes formed. This was done by measuring the temperature-dependent dissociation of pre-formed complexes taking advantage of TGGE analysis. Complexes of wild-type and T11 mutant leader transcripts with the 5′ 16S rRNA fragment were formed and separated on the same TGGE gel at slightly different loading times. A temperature gradient was established between 10 and 25°C. Following electrophoresis the temperature at which 50% of the initial complex dissociated (T_m) was determined. The T_m values obtained in this way did not differ by >1°C for the wild-type (T_m = 16.8°C) and the T11 mutant (T_m = 17.8°C), but are consistent with the measured binding affinities (data not shown).

To determine whether higher order RNA structural elements might be involved in the leader–16S rRNA interaction we analyzed the Mg^{2+} dependence of complex formation between leader transcripts and the 16S rRNA 5′-domain. Mg^{2+} concentrations were varied between 0 and 10 mM and complex formation was monitored with the standard gel retardation assay (Fig. 3a). Apparent binding constants were derived by quantifying the intensities of complexes and the free fragment from several experiments (24). The results are summarized in Figure 3b. In accordance with a slightly higher binding constant for the T11 mutant leader (Table 2) the analysis revealed that the T11 leader had a higher affinity for 16S rRNA which is rather constant throughout the range of Mg ion concentrations tested. In contrast, the Mg^{2+} ion dependence for complex formation with the wild-type leader shows a biphasic behavior. There is no significant difference in binding constants for Mg^{2+} ion concentrations between 0.1 and 1 mM. Above 1 mM there is a rather sharp increase in binding constants however, indicative of a Mg-dependent cooperativity. One could infer from the results that the mutant leader might not be folded in the same tight or compact structure such that potential interacting sequences are more easily accessible for 16S rRNA complex formation.

In summary, we corroborated the observation that the interaction between the leader RNA and the nascent 16S rRNA is almost certainly restricted to the 5′-domain of the 16S molecule. This interaction appears to be of a transient nature since subsequent formation of the RNase III processing stem, which involves leader and spacer sequences, is not disturbed. Small differences in the affinities and stabilities of the mutant and wild-type leaders in complexes with the 16S 5′-domain can be measured. The Mg^{2+}-dependent differences in complex formation of mutant and wild-type leaders with the 16S rRNA are indicative of a less stably structured leader as a result of the base change mutations. The resulting, probably more open, structure might be responsible for a higher stability of the transient complexes formed with the nascent 16S rRNA.

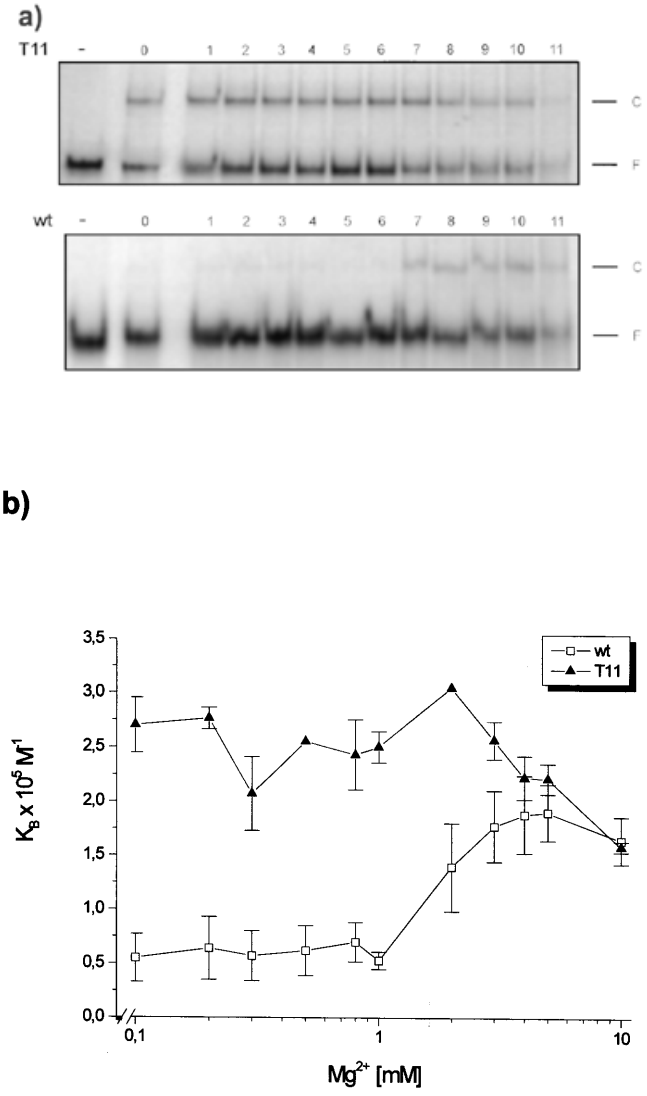

Figure 3. Mg^{2+}-dependent complex formation of the 5′ 16S RNA domain with different leader RNA species. (**a**) T11 mutant (T11) and wild-type leader (wt) transcripts, 1.5 µM each, were subjected to complex formation with 100 nM ^{32}P-labeled 5′ 16S RNA transcript. The following Mg^{2+} concentrations were employed: 0 (lane 0), 0.1 (lane 1), 0.2 (lane 2), 0.3 (lane 3), 0.5 (lane 4), 0.8 (lane 5), 1 (lane 6), 2 (lane 7), 3 (lane 8), 4 (lane 9), 5 (lane 10), and 10 mM Mg^{2+} (lane 11). The lane indicated by – represents the control without leader at 1 mM Mg^{2+}. (**b**) The apparent binding constants for the formation of leader RNA–16S rRNA complexes derived from several experiments as shown in (a) are presented as a function of Mg^{2+} concentration.

Is 16S rRNA folding affected by the presence of leader sequences?

As opposed to formation of the structure of double helical DNA the folding of complex RNA molecules occurs in discrete steps where the individual transitions are considered to reflect a hierarchical order. At first two- and three-dimensional elements are formed by sequence-dependent interactions of nucleic acid bases. These merge into structural units that fold separately along the polynucleotide backbone. The tertiary structure is then formed by the association of pre-folded domains. Pre-folding and tertiary structure formation is completed by the interaction of cations (e.g. Mg^{2+}) and/or proteins (25–27). Our understanding of the complex kinetic steps in the folding pathway is relatively limited and only a small number of small RNA molecules have been studied in detail. In order to find out whether kinetic steps during the folding pathway leading to mature 16S rRNA might be affected by sequence changes in the leader we established an oligonucleotide hybridization assay and monitored the folding

times of selected RNA regions. The assay is based on a procedure described recently (19). In this procedure the time-dependent change in the accessibility of a folding structure is determined by the change in the rate of complementary oligonucleotide binding. Hence, oligonucleotides directed against crucial sequence regions of the RNA target molecule are used as structural probes. Binding of the oligonucleotides is monitored over time starting from the unfolded (thermally denatured) target RNA. The time-dependent change in hybridization with specific oligonucleotides is then quantitated. To this end, hybridization signals are determined as a function of time after the onset of renaturation as described in Materials and Methods. In a simple case of secondary structure (helix) formation from a single-stranded sequence the time-dependent decrease in the hybridization signal is characteristic for the folding time and half-lives of helix formation can be readily derived from this determination. In comparable studies with RNase P (28) and group 1 ribozymes (29) and the folding of mRNA secondary structures (19) folding times in the range of seconds to minutes have been determined. It appeared reasonable, therefore, to expect at least some folding events for the 16S rRNA structure to occur on the same time scale.

The hybridization experiments were performed with 16S rRNA transcripts that either contained no leader, the wild-type leader or the T11 mutant leader. Oligonucleotides were chosen that were complementary to selected structural elements of the 16S rRNA (Materials and Methods). The locations of the regions of complementarity for the individual oligonucleotides used are indicated in Figure 5. The RNA molecules were denatured and subsequently aliquots of the solution were mixed after distinct time intervals with equal amounts of radiolabeled oligonucleotides together with a recovery marker. Time intervals of 0, 10, 20, 30, 60 and 120 s were chosen. Hybridized samples were separated on composite agarose–acrylamide gels at 4°C and hybridization signals were quantitated by densitometry of the corresponding autoradiograms. Examples from two such gels representing the folding of 16S rRNA helices 3 and 6 are exemplified in Figure 4a. Figure 4b shows the quantified data for six different oligonucleotides complementary to helices 3, 6, 8, 20, 31 and 44. Helix numbering of the 16S rRNA is according to Brimacombe *et al*. (18). The locations of the different helices within the 16S rRNA secondary structural model are presented in Figure 5. It can be seen that the hybridization signals for helix 6 decrease in an exponential way for all the different transcripts tested. This allows the derivation of folding half-lives for the formation of helix 6 which differ significantly when the leader RNA is absent or when it contains base changes. The presence of the wild-type leader clearly reduces the folding rate of helix 6 compared to the leader-less transcript (24 versus 12 s), while the presence of the T0 mutant leader results in about the same folding half-life as for the leader-less transcript. The corresponding folding half-lives are presented in Table 3. Note that helix 6 has been shown by cross-linking to be in direct contact with the leader (13). As opposed to the simple kinetic behavior of helix 6, the folding of helix 3, for instance, is more complex. This is at least true for the transcripts that contain no leader or the wild-type leader. The hybridization curves appear biphasic with a rapid increase in oligonucleotide binding within the first 20 s, followed by a slow decrease over ~1 min. This complex folding very likely reflects the fact that helix 3 results from long range interactions and may be formed from (one or more) structural intermediates that are rate limiting. It should be emphasized that helix 3 is very important in folding of the 16S rRNA and the folding kinetics of the mutant leader may probably be related to the cold-sensitive phenotype. Helix 3, through long range interactions, links the complex rRNA 3′-domain, which is important for the early assembly steps, to the central rRNA pseudoknot formed by helices 1 and 2. Long range interactions do not generally cause a complex folding kinetic however. This is evident for helix 20, for instance, where the folding of the intermediate sequences are apparently not rate limiting. Helix 20 shows again a simple exponential decrease in binding. Differences in the leader do not significantly affect the folding half-lives for this helix (Table 3). Complex folding kinetics can be seen for helices 8 and 31 (note, however, that folding of helix 8 is actually too fast to be accurately determined with the hybridization assay). In these cases either transient intermediate structures or tertiary interactions may be responsible for the complex hybridization behavior. At some sites, e.g. helix 44, folding times of the RNA secondary structure appear either to be too fast to allow a meaningful change in hybridization to the complementary oligonucleotide or the oligonucleotide cannot form a stable hybrid for other reasons. This applies also to helices 17 and 18. Repeated attempts to characterize the formation of these helices with our assay failed and we could not detect measurable hybridization signals under our experimental conditions. It is possible that structure formation for these helices is too fast to be measured or, more likely, that the corresponding structures do not melt during the denaturation step. No data for helices 17 and 18 are included in Figure 4b, therefore.

Table 3. Folding times for 16S rRNA secondary structural elements

16S rRNA position	$t_{1/2}$ (s)		
	No leader	Wild-type leader	T11 leader
Helix 6 (66–82)	11.9	23.7	13.2
Helix 20 (572–587)	26	25	24.1

In summary, although only a limited number of 16S rRNA structural elements were tested by the hybridization assay, the study revealed clear differences in folding times for some 16S rRNA positions, depending either on the presence of the leader or on base changes within the leader. Differences are most pronounced for structural elements close to the 16S rRNA 5′-end.

Taken together we have shown in this study that rRNA leader sequences are able to form intermediate complexes with the 5′-domain of the growing 16S rRNA transcript. The stability of the complexes formed is affected by base changes in the leader that have been shown to confer a cold-sensitive phenotype. Moreover, the folding kinetics of defined 16S rRNA regions are altered by the presence of the leader or by base changes within the leader. The study thus corroborates earlier findings that the leader sequence has an important function in the folding and maturation process that leads to functional 30S ribosomes. It furthermore extends our knowledge indicating that both thermodynamic and kinetic steps are involved in this interesting mechanism. The results are consistent with the view that the leader seems to protect sequence regions from folding

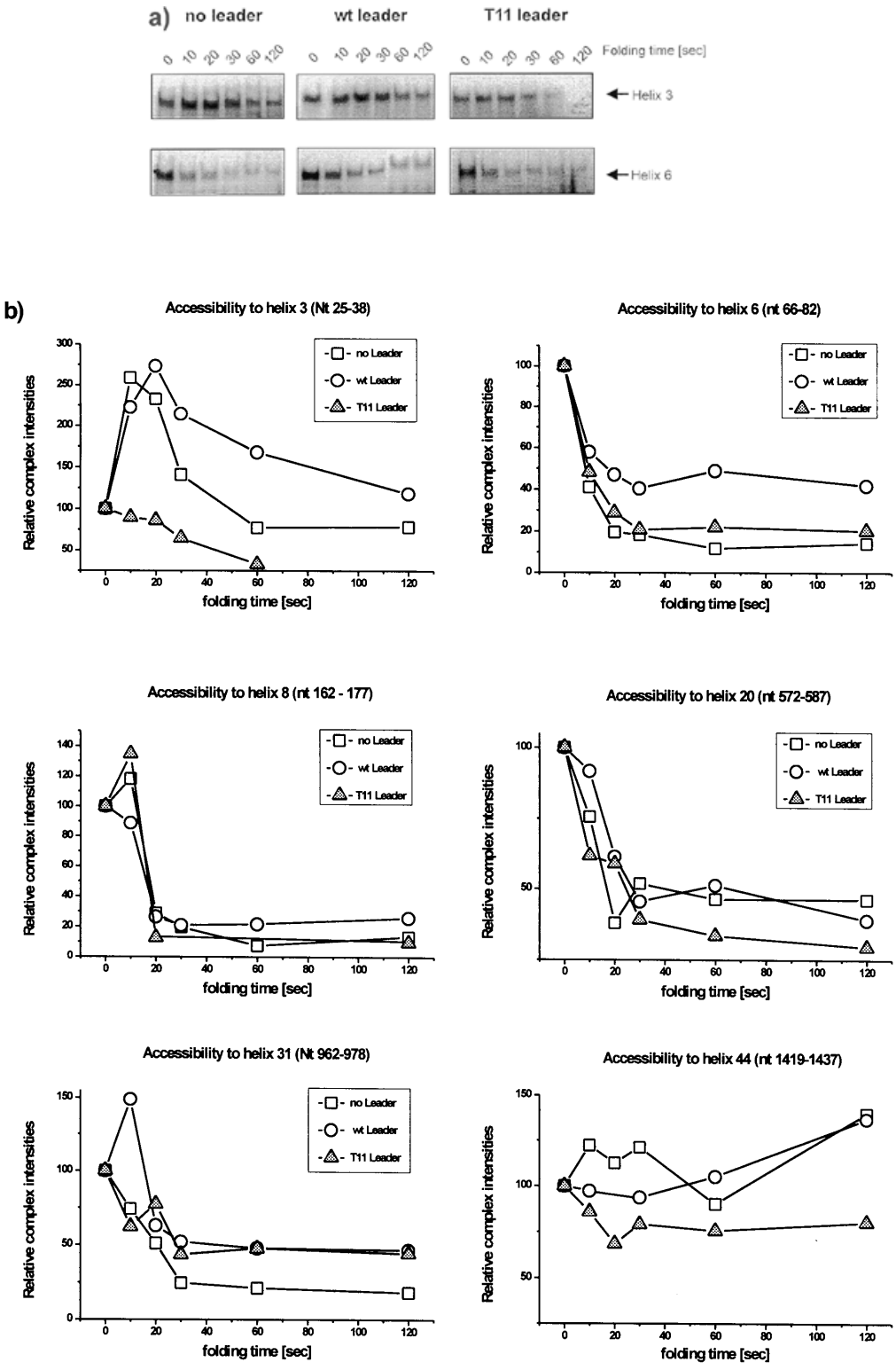

Figure 4. Oligonucleotide hybridization analysis to monitor 16S rRNA folding kinetics. (**a**) The time-dependent complex formation of two oligonucleotides directed to the 16S rRNA secondary structure elements (helix 3 and helix 6) is exemplified for 16S rRNA transcripts without leader (no leader) or with wild-type or T11 mutant leader (wt leader or T11 leader, respectively). Folding times in seconds are indicated. (**b**) The relative band intensities of oligonucleotide–16S rRNA complexes from several experiments as shown in (a) are plotted as a function of the folding time. In each panel the respective helix which was probed by the individual oligonucleotide is given in the headline. Different symbols are given for the 16S rRNA transcripts that either contain no leader (squares) or wild-type (circles) or T11 mutant leader (triangles). The folding times are indicated in seconds.

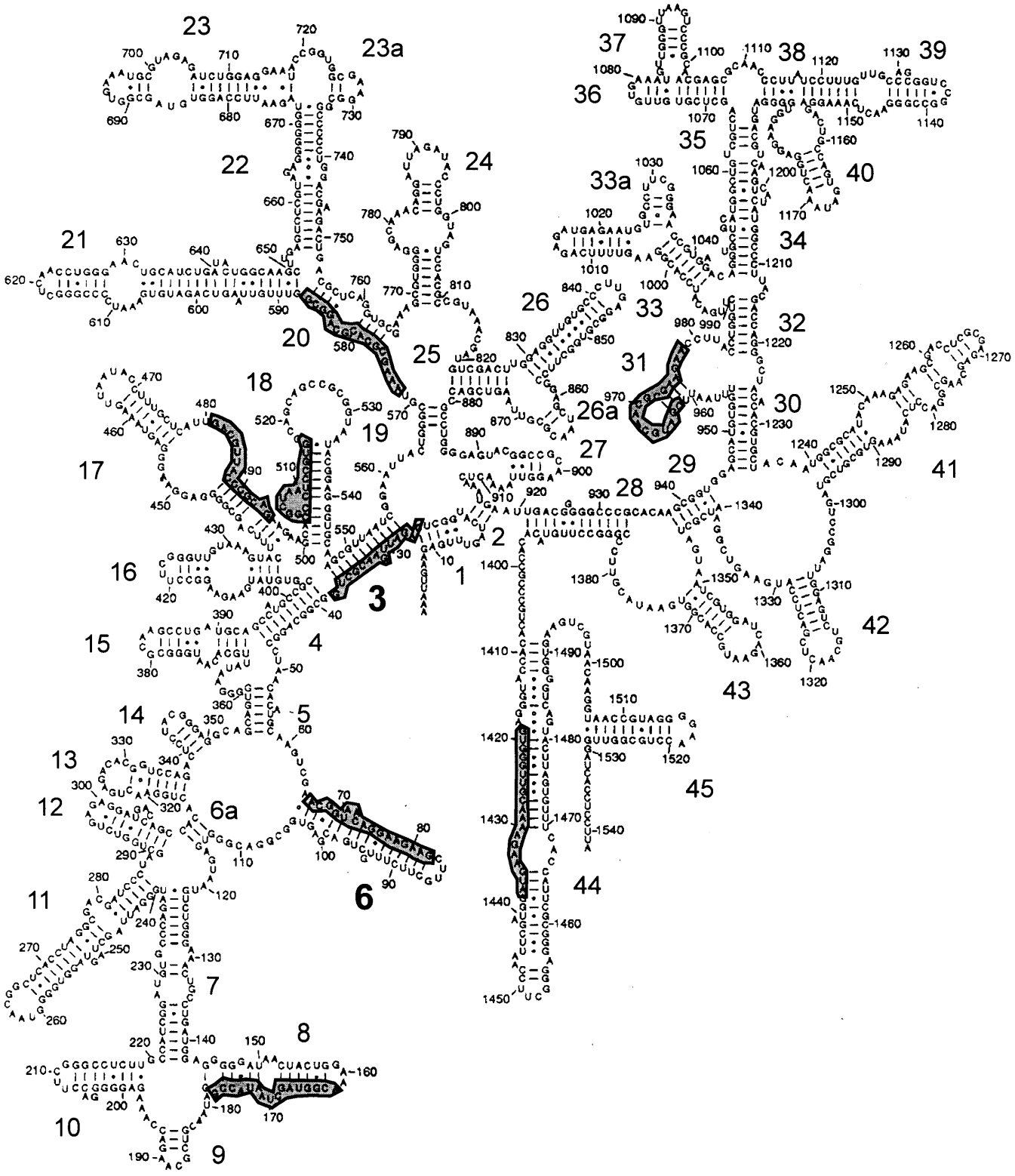

Figure 5. Location of the secondary structural elements probed by the oligonucleotide hybridization assay. Sequence regions against which complementary oligonucleotides had been directed are outlined in dark shaded boxes. The different helices are indicated by numbers. Helices 3 and 6, which are most strongly affected by different leader sequences, are outlined in bold. Helix numbering is according to Brimacombe *et al.* (18). The secondary structure model has been taken from Stern *et al.* (33).

into irreversible structures by forming transient intermediates with early transcribed regions of the 16S rRNA. If the leader cannot form these metastable intermediates the folding pathway may generate incorrect structures that are too stable to be converted to the final structures at limiting temperatures. Defective structures may thus get trapped and give rise to malfunctioning ribosomes. A similar function is discussed for the eukaryotic U3 snoRNAs which also support structure formation and correct processing of eukaryotic small subunit rRNAs (30–32).

Finally it should be noted that we have concentrated in this study on effects that depend directly on the thermodynamics and kinetics of RNA–RNA interaction. We certainly do not rule out the participation of proteins during the complex folding process *in vivo*. Binding of the Nus proteins NusA, NusB and probably NusG as well as the ribosomal protein S10 to the leader *nut*-like elements suggests that the chaperone-like activity of the leader RNA in guiding formation of functional 30S subunits might in addition be supported by these proteins.

ACKNOWLEDGEMENTS

We would like to thank Dr S. Mundt, Dr G. Steger, Dr R. Lück and Dipl. Biol. O. Schrader for their advice on UV melting analysis and RNA structure computations. T7 RNA polymerase was a kind gift of B. Esters. This work was supported by grants from the Deutsche Forschungsgemeinschaft and by the Fonds der Chemischen Industrie

REFERENCES

1. Wagner,R. (1994) *Arch. Microbiol.*, **160**, 100–109.
2. King,T.C., Sirdeskmukh,R. and Schlessinger,D. (1986) *Microbiol. Rev.*, **50**, 428–451.
3. Srivastava,A.K. and Schlessinger,D. (1990) *Annu. Rev. Microbiol.*, **44**, 105–129.
4. Srivastava,A.K. and Schlessinger,D. (1989) *EMBO J.*, **8**, 3159–3166.
5. Mori,H., Dammel,C., Becker,E., Triman,K. and Noller,H.F. (1990) *Biochim. Biophys. Acta*, **1050**, 323–327.
6. Szymkowiak,C., Reynolds,R.L., Chamberlin,M.J. and Wagner,R. (1988) *Nucleic Acids Res.*, **16**, 7885–7899.
7. Liiv,A., Tenson,T., Margus,T. and Remme,J. (1998) *Biol. Chem.*, **379**, 783–793.
8. Balzer,M. and Wagner,R. (1998) *J. Mol. Biol.*, **276**, 547–557.
9. Young,R.A. and Steizt,J.A. (1978) *Proc. Natl Acad. Sci. USA*, **75**, 3593–3597.
10. Bolivar,F. and Backman,K. (1979) *Methods Enzymol.*, **68**, 245–267.
11. Marinus,M.G. (1983) *Mol. Gen. Genet.*, **192**, 288–289.
12. Sambrook,J., Fritsch,E.F. and Maniatis,T. (1989) *Molecular Cloning: A Laboratory Manual*, 2nd Edn. Cold Spring Harbor Laboratory Press, Cold Spring Harbor, NY.
13. Pardon,B. and Wagner,R. (1995) *Nucleic Acids Res.*, **23**, 932–941.
14. Pardon,B. (1994) PhD thesis, Heinrich-Heine-Universität, Düsseldorf, Germany.
15. Brosius,J., Dull,T.J., Sleeter,D.D. and Noller,H.F. (1981) *J. Mol. Biol.*, **148**, 107–125.
16. Pardon,B., Thelen,L. and Wagner,R. (1994) *Biol. Chem. Hoppe Seyler*, **375**, 11–20.
17. Rosenbaum,V. and Riesner,D. (1987) *Biophys. Chem.*, **26**, 235–246.
18. Brimacombe,R., Atmadja,J., Stiege,W. and Schüler,D. (1988) *J. Mol. Biol.*, **199**, 115–136.
19. Ma,C.K., Kolesnikow,T., Rayner,J.C., Simons,E.L., Yim,H. and Simons,R.W. (1994) *Mol. Microbiol.*, **14**, 1033–1047.
20. Steger,G., Hofmann,H., Förtsch,F., Gross,H., Randles,J.W., Sänger,H.L. and Riesner,D. (1984) *J. Biomol. Struct. Dyn.*, **2**, 2760–2768.
21. Steger,G. (1994) *Nucleic Acids Res.*, **22**, 2760–2768.
22. Schmitz,M. and Steger,G. (1992) *Comp. Appl. Biosci.*, **8**, 389–399.
23. Theißen,G., Thelen,L. and Wagner,R. (1993) *J. Mol. Biol.*, **233**, 203–218.
24. Carey,J. and Uhlenbeck,O.C. (1983) *Biochemistry*, **22**, 2610–2615.
25. Brion,P. and Westhof,E. (1997) *Annu. Rev. Biophys. Biomol. Struct.*, **26**, 113–137.
26. Zarrinkar,P.P. and Williamson,J.R. (1994) *Science*, **265**, 918–924.
27. Draper,D.E. (1996) *Trends Biochem. Sci.*, **21**, 145–149.
28. Zarrinkar,P.P., Wang,J. and Williamson,J.R. (1996) *RNA*, **2**, 564–573.
29. Banerjee,A.R. and Turner,D.H. (1995) *Biochemistry*, **34**, 6405–6512.
30. Hughes,J.M.X. (1996) *J. Mol. Biol.*, **259**, 645–654.
31. Steitz,J.A. and Tycowski,K.T. (1995) *Science*, **270**, 1626–1627.
32. Dennis,P.P., Russell,A.G. and De Sa,M.M. (1997) *RNA*, **3**, 337–343.
33. Stern,S., Weiser,B. and Noller,H.F. (1988) *J. Mol. Biol.*, **204**, 447–481.